In-situ chemical, U–Pb dating, and Hf isotope investigation of megacrystic zircons, Malaita (Solomon Islands): Evidence for multi-stage alkaline magmatic activity beneath the Ontong Java Plateau

Antonio Simonetti *, Clive R. Neal

Department of Civil Engineering and Geological Sciences, 156 Fitzpatrick Hall, University of Notre Dame, Notre Dame IN 46556, USA

ABSTRACT

Previous investigations of pipe-like intrusions of alnöite within northern Malaita (Solomon Islands) have detailed the chemical and isotopic nature of the alnöite and entrained megacrysts/xenoliths. Alnöite emplacement is poorly constrained since available ages include an Ar–Ar date of 34 Ma (phlogopite) from a mantle xenolith, and a $^{206}Pb/^{238}U$ date of 33.9 Ma for a zircon megacryst. Hence, we report chemical data, in-situ U–Pb age determinations and Hf isotope compositions for megacrystic zircons recovered from alnöite-derived, ilmenite-rich gravels in the Auluta, Kwainale, and Faufaumela rivers of Malaita.

The Zr/Hf ratio (39 to 50) is variable for zircons from Auluta and Faufaumela, whereas it is relatively uniform (40 to 42) in most zircons from Kwainale. Chemical imaging reveals the homogeneous nature for all of the 16 grains analyzed. Trace element compositions obtained by LA-ICP-MS indicate parallel chondrite-normalized REE patterns at variable levels of enrichment; these patterns combined with their low abundances (<1 to 10 ppm) of U, Th, and Pb confirm their mantle origin. In-situ U–Pb dating conducted by LA-ICP-MS ($n = 94$ analyses) define a total range in weighted mean (WM) $^{206}Pb/^{238}U$ ages between ~35 and ~52 Ma. The zircons from Auluta define a range of WM $^{206}Pb/^{238}U$ ages between 34.9 ± 2.0 Ma and 45.1 ± 2.5 Ma (2σ) that correlate negatively with Zr/Hf ratios and total REE contents. Conversely, the chemically homogeneous zircons from Kwainale define a uniform age spectrum yielding a WM $^{206}Pb/^{238}U$ age of 36.7 ± 0.5 Ma (2σ). In-situ Hf isotope analyses ($n = 30$) are uniform and define a WM $^{176}Hf/^{177}Hf$ value of 0.282933 ± 0.000013 (2σ), which is identical to the previously reported whole rock value for the Malaitan alnöite (0.282939 ± 0.000007). Correlations between ages and chemical compositions (i.e., Auluta zircons), and the uniform Hf isotope compositions are consistent with zircon formation from a common Ontong Java Plateau (OJP)-like mantle undergoing progressive CO_2-dominated metasomatism over a ~17 Ma interval. This unique example of prolonged highly alkaline magmatism within an intraplate oceanic setting mimics that defined by cratonic kimberlite provinces and suggests that the Malaitan upper mantle section of the OJP represents an analogy to continental lithosphere.

© 2010 Elsevier B.V. All rights reserved.

1. Introduction

The Solomon Islands chain is located within the southwestern Pacific region and delineates the boundary between the Pacific and Indo–Australian lithospheric plates (Fig. 1). The region is dominated by the Ontong Java Plateau (OJP; Fig. 1), which is a vastly over-thickened area of oceanic crust (a maximum crustal thickness of >30 km has been reported by Coffin and Eldholm, 1994; Gladczenko et al., 1997; Richardson et al., 2000; Miura et al., 2004), and is adjacent to the Indo–Australian plate. The exact origin of the OJP remains the subject of much debate and is beyond the context of this study.

The Soloman Islands were subdivided into three geological provinces (Coleman, 1965; Petterson et al., 1999): The Pacific Province (includes the island of Malaita — Fig. 1B), the Central Province, and the Volcanic Province. Islands located within the Pacific Province are characterized predominantly by Late Mesozoic basement (based on paleontological evidence from overlying sediments) consisting of unmetamorphosed oceanic basalts (Hughes and Turner, 1976). The island of Malaita (Fig. 1B) is geologically distinct from the remaining islands of the Solomons Chain since it represents the southwestern border of the OJP.

According to Petterson (1995) and Petterson et al. (1999), the geology of Malaita (Fig. 1B) can be summarized as follows: The basement consists of mono-lithological Cretaceous basalt sequence up to 4 km thick and is termed the Malaita Volcanic Group (MVG). This basalt sequence has yielded Ar–Ar plateau ages of between 125 and 121 Ma, and is immediately overlain by the Lower to Mid-Cretaceous
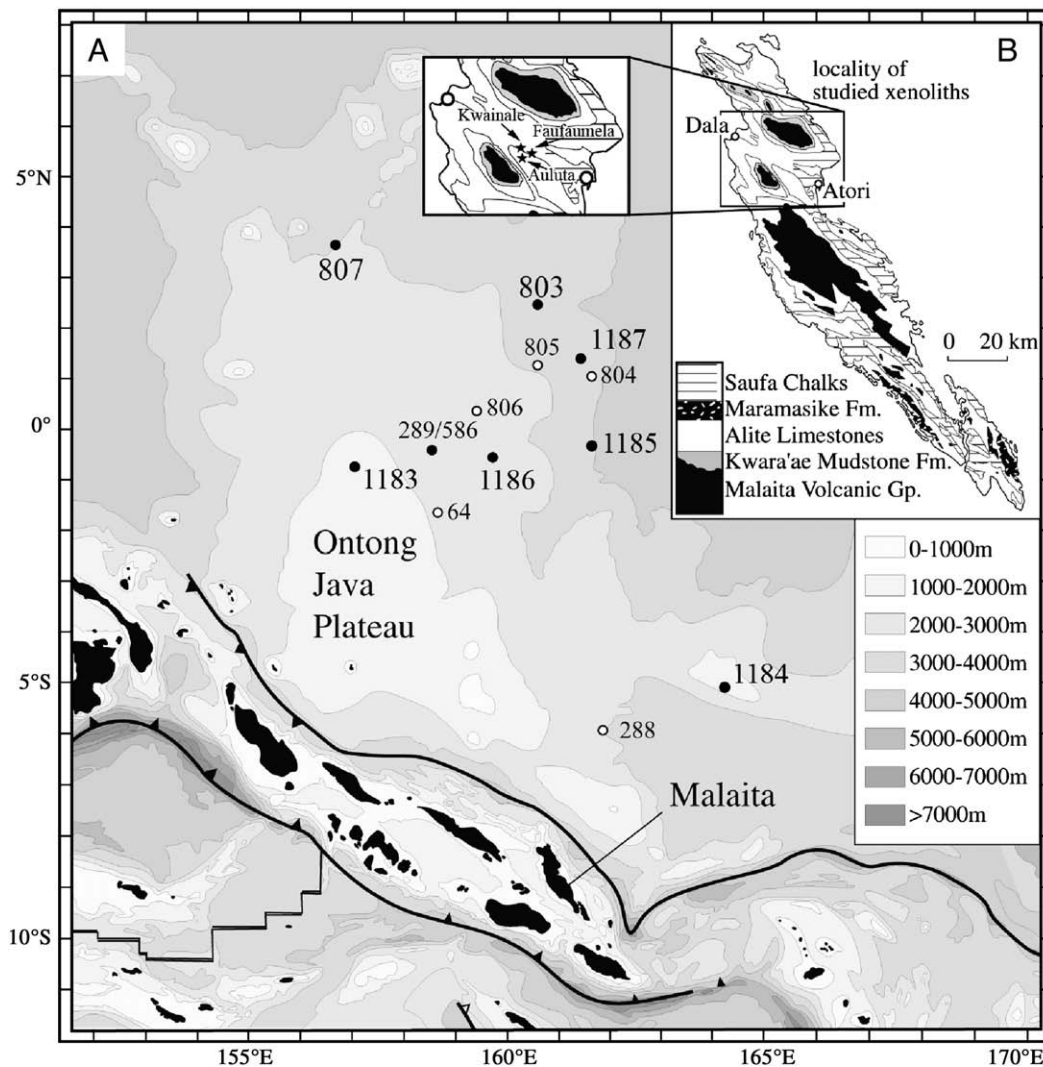
Fig. 1. A) Bathymetric regional map of the main part of the Ontong Java Plateau and location of Solomon Islands volcanic arc chain (modified after Ishikawa et al., 2004). Numbered sample locations within OJP indicate ocean drilling program (ODP), with solid circles representing sites that have intersected basement. B) Inset illustrates simplified geological map of Malaita (after Petterson, 1995) indicating sample locations.

Kwaraae Mudstone Formation (100–270 m thick). This is then conformably overlain by the Alite Limestone Formation (Mid-Cretaceous to Lower Eocene), which consists of alternating sequence of very fine-grained foraminiferal calcilutites with regularly interbedded chert. The Alite Formation is overlain by highly brecciated and vesicular alkaline basalts of the Maramasike Formation. One sample from this volcanic formation has yielded an Ar–Ar plateau age of 44.2 ± 0.2 Ma (Tejada et al., 1996). The Eocene to Mid Miocene Haruta Limestone Formation conformably overlies the Alite Limestone, and locally the Maramasike Volcanic Formation. This package was punctuated by alkaline basalt volcanism during the Eocene and intrusion of ultramafic alnöites during the Oligocene. The alnöite breccia and fine-grained pipes and sills intrude the Malaitan cover sedimentary sequence as high as the Lower Haruta Formation levels (i.e. mid-Eocene, ~44 Ma). The basement and cover sequences were later deformed by an intense but short deformation event during the mid-Pliocene. There are localized occurrences of Upper Pliocene–Pleistocene shallow marine to subaerial formations that overlie the Mid-Pliocene unconformity surface.

The occurrence of pipe-like bodies, which resemble volcanic plugs, has been documented by seismic refraction studies at the northeastern periphery of the OJP (Nixon, 1980). On the island of Malaita, samples of alnöite were subsequently discovered and described (Allen and Deans, 1965) as ultramafic lamprophyres, which are character-

ized by the occurrence of essential melilite and no feldspar (Rock, 1986). The pipe-like bodies of alnöite were explosively emplaced into limestones and mudstones that have been folded into NW–SE trending anticlines and synclines (Petterson, 1995). The location of the alnöite intrusions are closely controlled by extensional faults/graben structures, which were active in central North Malaita from at least the Eocene to the Lower Pliocene (Petterson, 1995). The alnöite intrusions are situated within the Auluta Thrust Belt-Faufaumela Basin area and Petterson (1995) indicates that this spatial/structural correlation is not fortuitous. The Auluta-Faufaumela region records an Eocene–Pliocene extensional phase that led to the formation of the graben structures. According to Petterson (1995), these structures facilitated the influx of alkaline basalt and alnöite magmas during the Eocene and Oligocene periods, and also permitted the accumulation of thick sediment deposits. Paleo-reconstruction of tectonic plate movements within the southwest Pacific basin indicates that alnöite emplacement occurred within an intraplate setting (Ishikawa et al., 2007) and hence not related to present-day subduction occurring along the Solomon Islands convergent zone (Fig. 1).

The alnöite pipes at Babaru'u and Kwaikwai are characterized by a black, fine-grained matrix with megacrysts surrounded by an autholithic breccia containing xenoliths of peridotite and country rock, megacrysts, and xenocrysts. Neal and Davidson (1989)

conducted a detailed petrographic, geochemical, and isotopic investigation of the megacryst suite and host Malaitan alnöite, which is silica-undersaturated (35.7 to 36.4 wt.% SiO_2) and olivine and nepheline normative. The megacryst suite consists of augite, subcalcic diopside, bronzite, garnet, ilmenite, and phlogopite, with each mineral defining a relatively large compositional range. Based on the geochemical and radiogenic isotope results for the alnöite and associated megacrysts, Neal and Davidson (1989) advocated for a petrogenetic model summarized here. It involves diapiric upwelling of a melt deep within a LREE-depleted asthenospheric mantle. The diapiric melt subsequently underwent zone refinement as it rose resulting in an alkali basaltic magma. The melt then impinged on the rigid lithosphere where it began to cool; this initiated fractionation of the megacryst suite. A subducted derivative of oceanic crust that is underplating the OJP is then assimilated by the *proto-alnöite* magma during megacryst fractionation (AFC process). The resultant alnöite is therefore the product of zone refining, fractional crystallization, and crustal assimilation.

To date, geochronological information for delineating the timing of alnöite emplacement within the magmatism associated with the entire OJP is scarce and is essentially defined by a single, non-constrained $^{206}Pb/^{238}U$ age of 33.9 Ma for a zircon megacryst obtained by thermal ionization mass spectrometry (Davis, 1978). Noteworthy is the fact that this age was not reported with an associated uncertainty; crucial information given that these young, mantle-derived zircon megacrysts are characterized by both low contents of radiogenic Pb ($\ll$1 ppm) and U ($\sim$5.0 ppm; Davis, 1978, and this study). Consequently, as noted by Davis (1978), calculation of the ^{207}Pb abundance results in large uncertainties associated with the $^{207}Pb/^{206}Pb$ and $^{207}Pb/^{235}U$ age determinations and these are therefore less significant. In contrast, the radiogenic ^{206}Pb content is more abundant resulting in $^{206}Pb/^{238}U$ ages that are much more robust and reliable. Kitajima et al. (2008) also reported a weighted mean $^{206}Pb/^{238}U$ age of 36.89 $\pm$ 0.41 Ma ($n = 23$ analyses) obtained by ion microprobe for zircons extracted from 1.5 kg of Malaitan alnöite (location within Malaita is not published). However, it is important to note that individual U–Pb ages reported by Kitajima et al. (2008) are characterized by very large associated uncertainties (up to 80% relative standard error), and the zircons investigated were submillimeter in size and much smaller than the millimetric-to-centimeter-sized zircon megacrysts investigated here (Fig. 2).

This study consists of a detailed, in-situ chemical, $^{206}Pb/^{238}U$ age dating, and Hf isotope investigation of 16 zircon megacrysts obtained from ilmenite-rich gravel deposits within the Auluta, Kwainale, and Faufaumela rivers of central northern Malaita (Fig. 1B). Zircon megacrysts were later recovered from these gravel samples by fluorescence using a UV (ultraviolet) lamp in a dark room. Major element characterization and chemical mapping (back scattered electron − BSE imaging) of the zircon megacrysts were conducted by using electron microprobe. In-situ trace element analysis, U–Pb age determinations, and Hf isotope ratios were all determined by laser ablation-inductively coupled plasma mass spectrometry (LA-ICP-MS). The main objectives of this investigation are to better constrain the emplacement age(s) of the alnöite pipes and evaluate various petrogenetic models, namely zone refinement + assimilation fractional crystallization (AFC) *versus* crystallization from discrete partial melting events, for the formation of the zircon megacrysts. Lastly, the chemical and Hf isotope data, and U–Pb age determinations are discussed in relation to the OJP and compared to similar-type alkaline magmatism that occurs in continental (cratonic) lithosphere.

2. Analytical methods

The major element compositions (ZrO_2, SiO_2, and HfO_2 wt.% abundances) of the Malaitan zircon megacrysts were measured using a JEOL8900R electron microprobe at the University of Alberta,

operated at 15 kV accelerating voltage and 20 nA probe current and 1 micron beam diameter. Data reduction was performed using the $\Phi(rZ)$ correction (Armstrong, 1995). The instrument calibration was deemed successful when the composition of secondary standards was reproduced within the associated uncertainties defined by the counting statistics. The major element compositions of the Malaitan zircon megacrysts are listed in Table S1.

In-situ trace element abundances and U–Pb age determinations reported here were obtained at the University of Notre Dame's LA-ICP-MS facility using a ThermoFinnigan high resolution Element2 ICP-MS instrument coupled to a UP213 laser ablation system from New Wave Research. Details with regards to the analytical protocols employed for the in-situ trace element analyses, U–Pb age determinations, and Hf isotope measurements are included within the Appendix. Table S2 lists the instrument operating conditions and outlines the data acquisition parameters used for determining trace element abundances (Table S1) and U–Pb ages (Table S3), and Table S4 contains the in-situ Hf isotope data.

3. Results

3.1. Chemical imaging and major and trace element compositions

Fig. 2 illustrates the megacryst zircon-bearing epoxy mounts and BSE images for several of the grains analyzed and these reveal homogeneous chemical compositions. Of the 16 grains investigated, none exhibited zoning, compositional banding, and/or evidence for the presence of inherited components. The latter feature has important implications for the U–Pb dating results. As reported for similar mantle-derived zircons, Schärer et al. (1997) also documented the lack of chemical zoning and compositional banding within zircon megacrysts from the Mbuji-Mayi kimberlite, Zaire.

Table S1 lists the major and trace element compositions of the Malaitan zircons investigated here. The ZrO_2 and SiO_2 abundances correspond to stoichiometric values of 67.2 and 32.8 wt.%, respectively. In contrast, HfO_2 values are quite variable in the Auluta (sample A-1) and Faufaumela (sample F-1) zircons defining ranges of 1.17 to 1.48 and 1.15 to 1.60 wt.%, respectively (Table S1). Individual zircon grains from Kwainale (sample K-1) are characterized by essentially homogeneous average HfO_2 contents of $\sim$1.40 wt.% (Table S1; $n = 10$ analyses for each grain; total range between 1.3 and 1.59 wt.%) with the exception of grain Z5 (average $HfO_2 = 1.20$ wt.%; values range between 1.12 and 1.35 wt.%). The corresponding Zr/Hf values range from $\sim$36 to $\sim$51 for both the Auluta and Faufaumela zircons, whereas the Kwainale zircons define rather uniform Zr/Hf values of $\sim$40 to $\sim$42 with the exception of grain Z5 ($\sim$48). Of interest is the fact that similar Zr/Hf values have been reported for zircons from the Bultfontein (Zr/Hf = 52) and Monastery (Zr/Hf = 39) kimberlites, South Africa (Heaman et al., 1990). Mitchell (1986) discusses the remarkable coherence in the Zr/Hf $\approx$ 45 for (whole rock) kimberlites on a world-wide basis that is independent of the age of emplacement. Moreover, a Zr/Hf value of 45 (Neal, unpublished data) was also obtained for whole rock alnöite sample CRN235 that was investigated as part of the Neal and Davidson (1989) study. Ishikawa et al. (2007) also report an average ($n = 5$ analyses) Zr/Hf value of 50 $\pm$ 10 for whole rock Malaitan alnöite.

In mantle-derived alkaline rocks, such as kimberlites and carbonatites, zircons are typically characterized by low total REE abundances (e.g., Hoskin and Schaltegger, 2003). For example, zircon from South African kimberlites contains total REE abundances that range between 5 and 39 ppm (Belousova et al., 1998), similar to those for zircon from carbonatites (e.g. Hoskin and Schaltegger, 2003); zircon from the MARID (mica–amphibole–rutile–ilmenite–diopside) suite is significantly more enriched in total REEs (average $\sim$640 ppm; Hoskin and Schaltegger, 2003). In contrast, zircon originating from crustal sources is characterized by variable and significantly higher total REEs
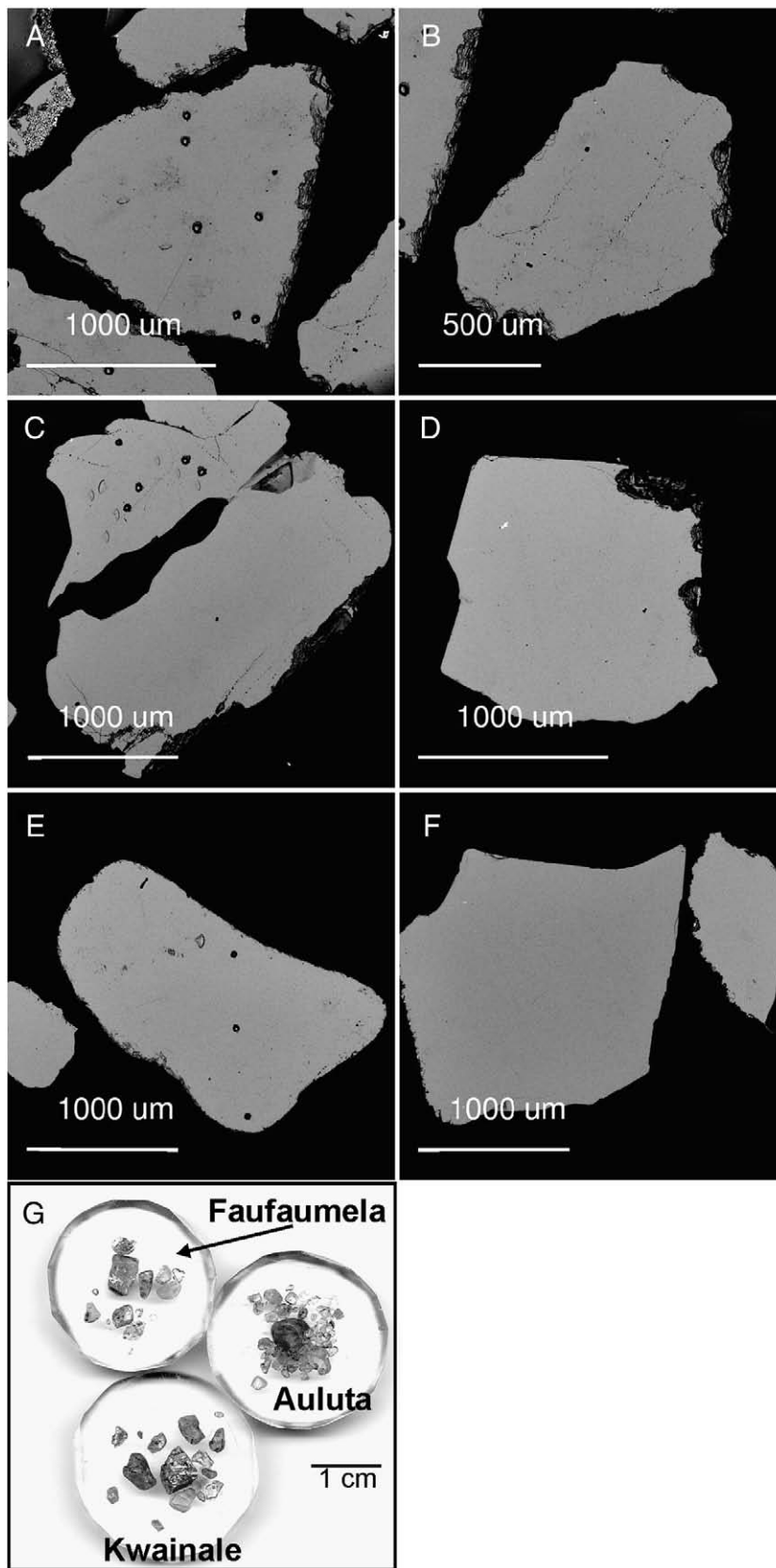
Fig. 2. Back scattered electron images of Malaitan zircon megacrysts: A- A1-Z3, B- A1-Z6, C- F1-Z1, D- F1-Z5, E- K1-Z1, F- K1-Z5. The small pits in several of the grains indicate locations of laser ablation spots (40 μm) for trace element analysis. G- Photo exhibiting the three epoxy mounts containing the megacryst zircon grains from Auluta, Faufaumela, and Kwainale.

contents (from ~250 to as much as ~5000 ppm) compared to mantle-derived zircon. The REE contents of the zircons investigated here ($n = 74$ analyses) are listed in Table S1; more than half of the analyses are characterized by REE contents <50 ppm (Fig. 3), which is similar to those reported for kimberlitic zircon megacrysts and confirms their mantle derivation. The average chondrite-normalized REE patterns for the three Malaitan zircon samples (Fig. 4) are almost identical with low LREE contents, positive Ce anomalies, and HREE normalized values varying between 10 and 100 times chondrite. Of interest, zircons from Auluta indicate a correlation between increasing Zr/Hf ratios and REE contents and $^{206}Pb/^{238}U$ age (Fig. 3), with grains containing lower REE abundances recording the older dates (i.e., Z4 and Z6).

Kimberlitic zircon megacrysts are also characterized by low U (<30 ppm) and Th (<10 ppm) contents and Th/U ratios of ~0.3 (Heaman et al., 1990; Zartman and Richardson, 2005), which in general are also features that characterize the Malaitan zircons investigated here (Table S1). An area of zircon grain F1-Z3 from the Faufaumela region is characterized by higher REEs, U, Th, and Pb contents compared to the remaining areas of the grain (Table S1; Fig. 4). This area within grain Z3 does not exhibit any variation in major element composition compared to the rest of the crystal. It is referred to as 'metasomatized'—'M' and also yields an artificially higher $^{206}Pb/^{238}U$ age of 59 ± 2.7 Ma (analysis F-1 Z3-3, Table S3b). Grain Z5 from sample F-1 also yields a similar, older WM $^{206}Pb/^{238}U$ age of 51.9 ± 2.6 Ma; however it is characterized by markedly lower abundances of REEs, Pb, Th, and U compared to the metasomitized area of grain Z3 (Tables S1 and S3b). This result clearly indicates that the oldest ages (>50 Ma) reported in this study are not strictly the result of metasomatic enrichment.

3.2. U–Pb dating results

Geochronological data obtained in this study are listed in Table S3 and shown in Figs. 5–7. As stated earlier, the $^{207}Pb/^{206}Pb$ and $^{207}Pb/^{235}U$ ratios (Table S3) are considered somewhat unreliable due to the extremely small ^{207}Pb ion signal as shown in Figs. 5A, 6A, and 7A; thus geochronological implications and interpretations are based solely on the WM $^{206}Pb/^{238}U$ values (ages). In several instances, the corresponding $^{207}Pb/^{206}Pb$ and $^{207}Pb/^{235}U$ ratios do yield concordant ages albeit these are associated with large uncertainties (Table S3).

The U–Pb data for the Auluta zircons are plotted in Fig. 5, and the consequence of the zircons having little ^{207}Pb as discussed above is clearly evidenced in the concordia plot (Fig. 5A). Fig. 5B illustrates the WM $^{206}Pb/^{238}U$ ages for individual zircon grains from the Auluta

Fig. 3. Plot showing variation of REEs vs. average Zr/Hf ratios for Malaitan zircon megacrysts. The zircon megacrysts from Auluta (solid circles) indicate a positive correlation between REEs and increasing Zr/Hf ratios and decreasing WM $^{206}Pb/^{238}U$ ages (data point labels), whereas the same parameters do not correlate with age determinations for the Faufaumela zircons (open circles).

region, and these range from 34.9 ± 2.0 Ma (2σ; grain Z3) to 45.1 ± 2.5 Ma (2σ; grain Z4) — a difference of ~10 Ma.

The concordia plot and WM $^{206}Pb/^{238}U$ ages for zircons from the Faufaumela region are shown in Fig. 6, and these range from 38.1 ± 1.7 Ma to 51.9 ± 2.6 Ma (2σ). The older age is defined by grain F-1 Z5, which is characterized by a low content of REEs (19 ppm), Th/U ratio of 0.26, and Zr/Hf ratio of ~36 (Table S1). One of the individual analyses (#3) from grain Z5 yields a concordant date of 50.7 ± 2.3 Ma (2σ; Table 3b). However, grain F-1 Z2 yields the youngest WM $^{206}Pb/^{238}U$ age at 38.1 ± 1.7 Ma (2σ; Fig. 6) but contains similar chemical characteristics compared to grain F-1 Z5 (the oldest grain); i.e. the lowest content of REEs (18 ppm), Th/U ratio of 0.37, and a Zr/Hf ratio of 36. Thus, unlike the coherent trends between the chemical data and U–Pb ages defined by the zircons from Auluta, those for the Faufaumela zircons are not as straightforward.

Fig. 7 illustrates the U–Pb analyses of the zircons from the Kwainale area on a concordia plot and WM $^{206}Pb/^{238}U$ age distribution diagram, respectively. Compared to the remaining samples, the 6 zircon grains from Kwainale indicate a rather uniform age distribution with several 'concordant' analyses for several of the grains analyzed (Table S3c). The total 33 analyses yield a weighted mean $^{206}Pb/^{238}U$ age of 36.72 ± 0.49 Ma (2σ; Fig. 7B).

3.3. Hf isotope results

The Hf isotope ratios (Table S4) obtained here for the Malaitan zircon megacrysts are plotted in a probability density plot (Fig. 8). The results listed in Table S4 indicate that the zircons record a homogeneous Hf isotope composition within individual grains, within each sample, and between the different samples, independent of the REE contents and the Zr/Hf ratio. The in-situ Hf isotope analyses define a WM $^{176}Hf/^{177}Hf$ value of 0.282933 ± 0.000013 (2σ; Fig. 8), which given the associated uncertainty is identical to the previously reported whole rock, average $^{176}Hf/^{177}Hf$ value of 0.282939 ± 0.000007 ($n = 5$) for the host alnöite (Ishikawa et al., 2007).

4. Discussion

4.1. Zircon megacryst formation — zone refinement and AFC versus discrete partial melting

The anhedral morphology and milli-to-centimeter grain size (Fig. 2), and major and trace element data reported here (Table S1) for the zircon samples from three central northern Malaita localities clearly indicate their mantle (deep-seated) origin. The Malaitan zircons are also characterized by a lack of chemical zoning and compositional variations (Fig. 2), which are also distinct features of megacrystic zircons derived from kimberlitic melts (e.g. Schärer et al., 1997). Mantle-derived zircon typically contains homogeneous textures with possible faint outlines of angular domains related to fracturing (Corfu et al., 2003). The lack or poor development of zoning in mantle-derived zircons may be related to prolonged residence of the megacrysts at high temperatures in the mantle (Corfu et al., 2003). This process may have led to partial or complete homogenization of any original zoning. This is suggested by the presence of a zone in Faufaumela crystal F1-Z3 that contains a higher abundance of trace elements although the major elements appear to be homogeneous throughout. Previous studies indicate that pre-eruptive residence times of kimberlitic and ultramafic lamprophyric melts in the upper mantle are short in duration (e.g., Kinny and Dawson, 1992; Kelley and Wartho, 2000). However, this may not always be the case as demonstrated by the variable U–Pb ages (~172 to ~2000 Ma old) reported for eclogitic mantle zircons from the Diavik kimberlite, Slave Province (Schmidberger et al., 2005), and centimeter-sized zircon megacrysts (~89 to ~106 Ma) from the Monastery kimberlite, South Africa (Zartman and Richardson, 2005).
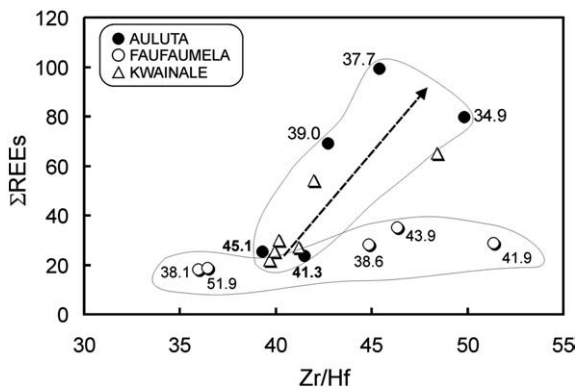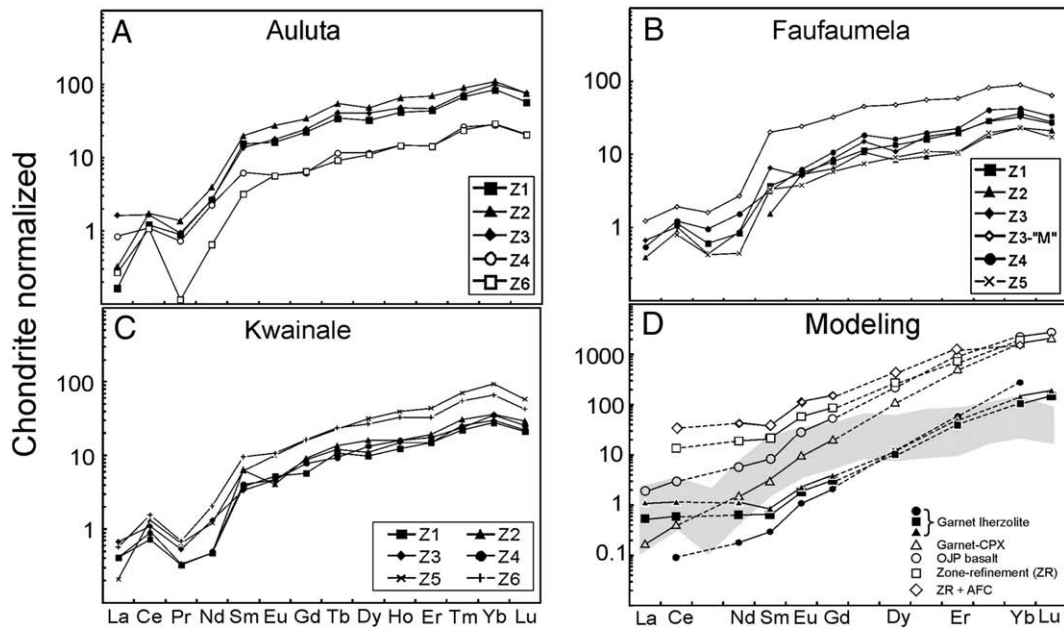
**Fig. 4.** Chondrite-normalized REE plots for zircons from (A) Auluta, (B) Faufaumela, and (C) Kwainale exhibiting the average compositions for all of the grains analyzed in this study (Table S1). Chondrite values are from Palme and Jones (2005). D) Plot illustrating the chondrite-normalized REE patterns for calculated zircon compositions in equilibrium with various melts/mantle source using the partition coefficients of Irving and Frey (1984). *Solid circle* = depleted asthenospheric mantle, *open square* = zone-refined melt, and *open diamond* = final alnöite melt subsequent zone refinement and fractional crystallization (all from Neal and Davidson, 1989); *open triangle* = clinopyroxene–garnet mantle xenolith from Ishikawa et al. (2007); *open circle* = OJP basalt from Mahoney et al. (1993); *solid square* = high-temperature garnet lherzolite and *solid triangle* = low-temperature garnet lherzolite from Schmidberger and Francis (1999) and Schmidberger et al. (2001). See text for detailed discussion.
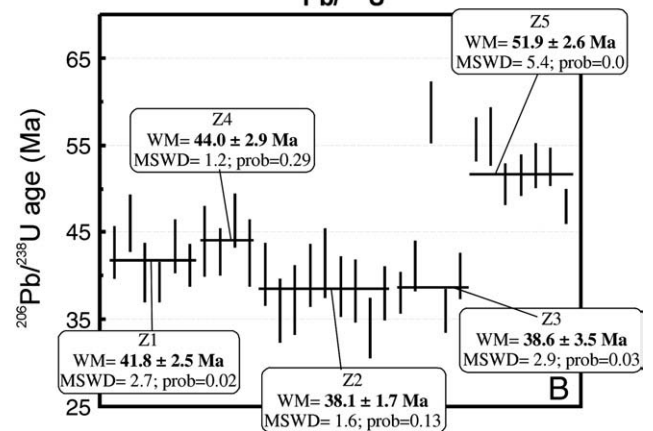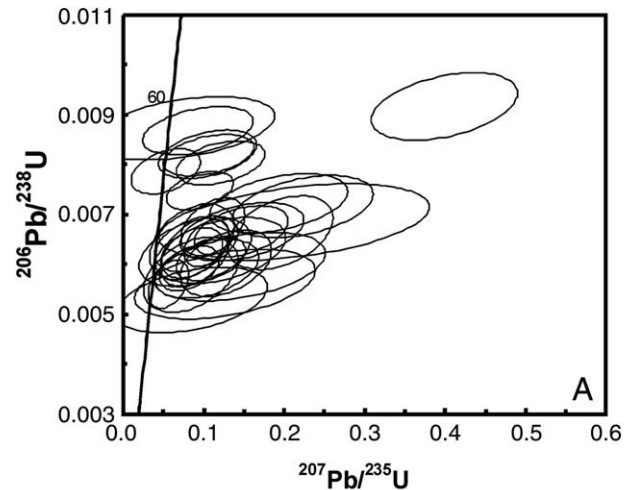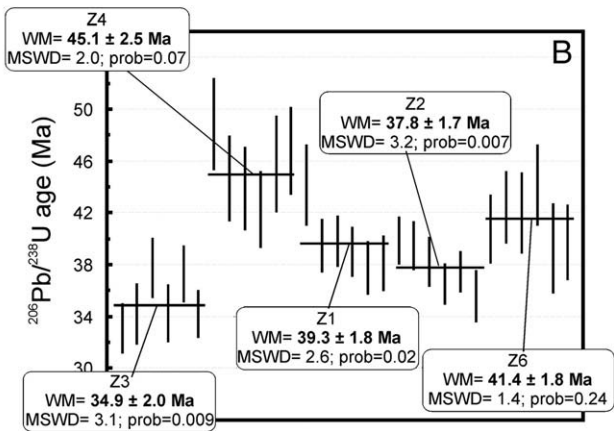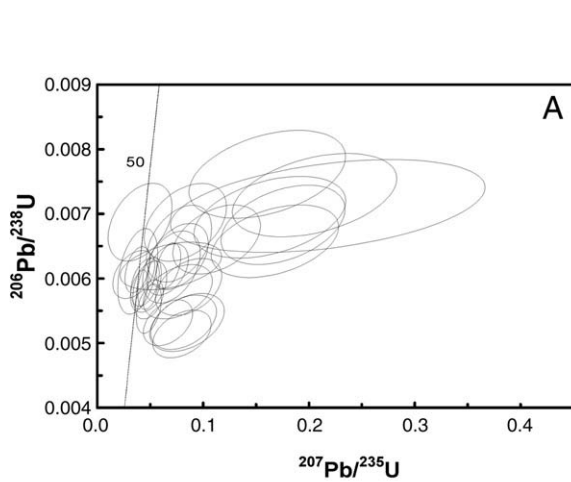
Fig. 5. A- Concordia plot showing the individual U–Pb laser ablation analyses for Auluta megacryst zircons analyzed (Table S3a); B- Diagram illustrating the distribution of the WM $^{206}Pb/^{238}U$ ages determined for individual Auluta zircon megacrysts. WM ages were calculated using IsoPlot/Ex3.00 (Ludwig, 2003).

Fig. 6. A- Concordia plot showing the individual U–Pb laser ablation analyses for Faufaumela megacryst zircons analyzed (Table S3b); B- Plot illustrating the distribution of the WM $^{206}Pb/^{238}U$ ages determined for individual Faufaumela zircon megacrysts. WM ages were calculated using IsoPlot/Ex3.00 (Ludwig, 2003).
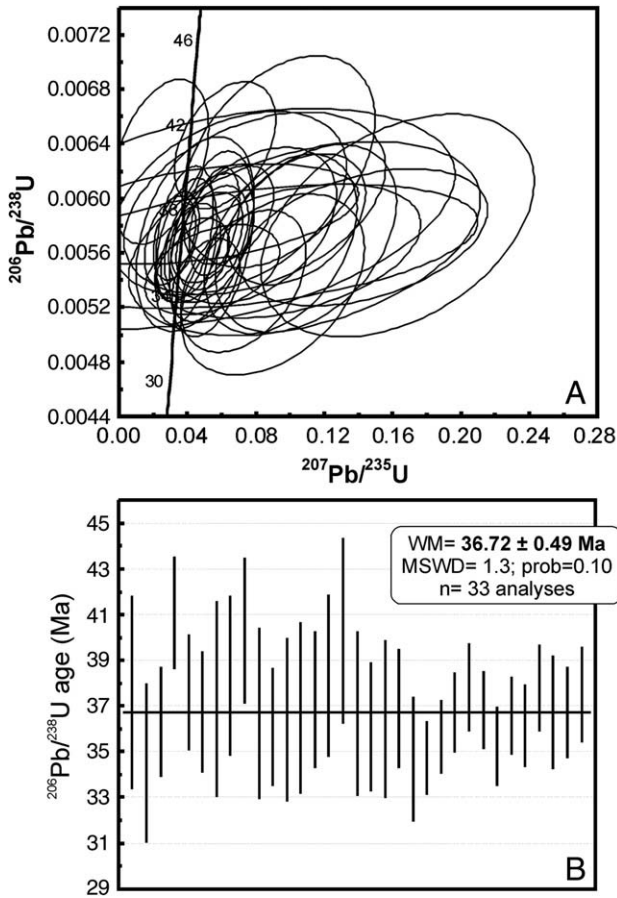
Fig. 7. A- Concordia plot showing the individual U–Pb laser ablation analyses for Kwainale megacryst zircons analyzed (Table S3c); B- Diagram illustrating the distribution of WM ^{206}Pb/^{238}U ages determined for individual Kwainale zircon megacrysts. WM ages were calculated using IsoPlot/Ex3.00 (Ludwig, 2003).

Th/U values for the Malaitan zircons investigated here range from 0.21 to 0.57 (Table S1), which overlaps the range of Th/U values (~0.2–1.0) recorded for both igneous zircons (Hoskin and Schalteg-ger, 2003) and those from kimberlites (e.g., Heaman et al., 1990; Konzett et al., 1998; Zartman and Richardson, 2005). Of importance, the chemical data for zircons from all three Malaitan samples (Table S1)
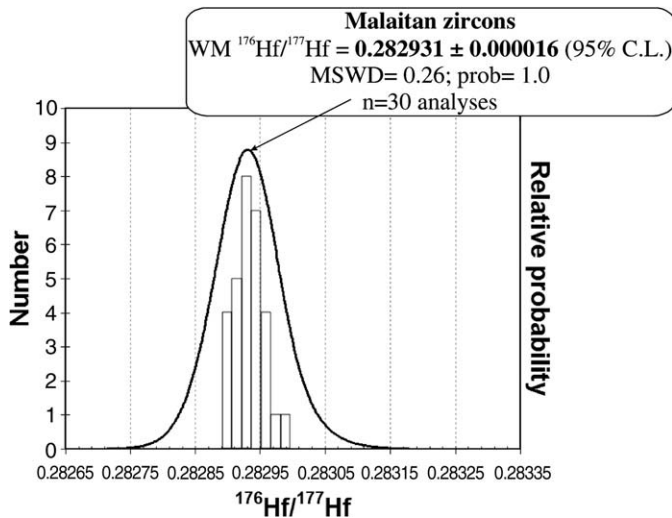
Fig. 8. Probability density plot illustrating the distribution of in-situ ^{176}Hf/^{177}Hf values obtained for Malaitan zircon megacrysts analyzed (Table S4). Plot and weighted mean calculations conducted using IsoPlot/Ex3.00 (Ludwig, 2003).

define nearly identical chondrite-normalized REE patterns (Fig. 4) and continuous trends in binary plots (e.g., Fig. 3). These may be indicative of crystallization from a common kimberlite-like magma or *proto-alnöitic* melt undergoing fractional crystallization (Neal and Davidson, 1989; Hoskin and Schaltegger, 2003). The chondrite-normalized patterns shown in Fig. 4 are HREE enriched (~10 to ~100 x chondrite), relatively flat to slightly positive HREE slopes with a positive Ce-anomaly, and lack negative Eu anomalies. Such features are consistent with igneous zircon, more specifically those derived from either kimberlitic (e.g. Hoskin, 1998) or carbonatitic melts (e.g. Mud Tank carbonatite; Currie et al., 1992; Hanchar and Hoskin, 1998).

Table S1 indicates that the Malaitan zircons are characterized by Zr/Hf ratios varying between ~36 and ~51, which range to values higher than primitive mantle (~36; Palme and O'Neill, 2005), depleted MORB mantle (DMM = 32.3; Workman and Hart, 2005) and continental crust (~36.3–38.7; David et al., 2000), but overlap those defined by zircons originating in kimberlites (39 to 58; Schärer et al., 1997; Heaman et al., 1990) and ocean island basalts (~37 to ~44; David et al., 2000). Jochum et al. (1986) argued that terrestrial rocks and chondrites were characterized by uniform Zr/Hf ratio of 36.6; with the major implication that there was essentially no relative fractionation between these two elements during magmatic processes such as partial melting or crystal fractionation. However, David et al. (2000) clearly demonstrated well-defined correlations between Sc abundances and Zr/Hf ratios for MORBs that are indicative of crystal fractionation involving clinopyroxene. This interpretation is consis-tent with results from experimental runs in basaltic systems that yielded higher clinopyroxene/liquid distribution coefficients for hafnium (D_{Hf} = 0.2 to 0.25) relative to zirconium (D_{Zr} = 0.1 to 0.14; Green, 1994; Lemarchand et al., 1987; Johnson, 1994; Skulski et al., 1994; Fujinawa and Green, 1997). Therefore, the correlation of increasing Zr/Hf ratios and REE contents with decreasing ^{206}Pb/^{238}U ages for the Auluta zircons (Figs. 3 and 9) may be attributed to melt differentiation involving fractional crystallization of clinopyroxene. With regards to the parental alnöite magma, there is clear evidence for crystal fractionation involving clinopyroxene since the latter occur as abundant megacrysts (Neal and Davidson, 1989). As stated earlier, based on the chemical and isotopic compositions of the various megacrystic suites and the host Malaitan alnöitic pipes, Neal and Davidson (1989) proposed an open system assimilation-fractional-crystallization (AFC) petrogenetic model. However, there is an important issue to consider when advocating for a model that invokes fractional crystallization at mantle depths in order to explain the negative correlation between age and Zr/Hf ratio exhibited by the Auluta zircons (Fig. 9); this process must have taken place over a ~10 Ma interval. As stated earlier, a prolonged residence time at upper
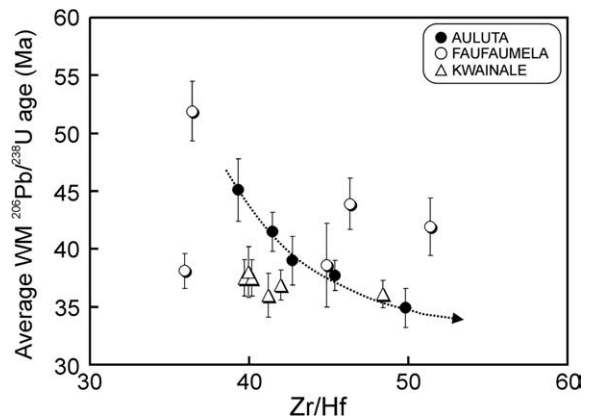
Fig. 9. Diagram illustrates the variation between average Zr/Hf values and calculated WM ^{206}Pb/^{238}U ages for Malaitan zircons. The negative correlation may reflect zircon formation form a mantle source undergoing progressive carbonate/CO_2-dominated metasomatism (see text for details).

mantle temperatures may explain the poor development of chemical zoning (Fig. 2); i.e. this scenario leads to partial or complete homogenization of any original zoning if present (Corfu et al., 2003). Of utmost importance is the lack of any correlation between Zr/Hf (and REEs) and decreasing WM ^{206}Pb/^{238}U ages for the Faufaumela megacrystic zircons (Figs. 3 and 9), which is also at odds with a petrogenetic model involving solely fractional crystallization.

We evaluate a possible origin via AFC for the generation of the Malaitan megacrysts zircons by calculating a series of zircon compositions based on available equilibrium REE partition coefficients for megacryst zircon crystallization in basaltic systems (Irving and Frey, 1984). In Fig. 4D, the range of the average chondrite-normalized REE patterns for the zircon megacrysts investigated here are compared to those for the calculated REE compositions for zircon in equilibrium with various parental melts/mantle sources. In particular, Fig. 4D illustrates the resultant chondrite-normalized REE patterns for zircon in equilibrium with mantle sources and melts present at the various stages of the combined asthenospheric diapiric melt, zone refinement (ZR), and AFC model of Neal and Davidson (1989). It is clear from the results shown in Fig. 4D that the calculated chondrite-normalized REE patterns for zircons in equilibrium with both the zone-refined and final alnöite (subsequent ZR + AFC) melts are too enriched compared to the range of measured chondrite-normalized patterns. Enriched REE contents (and chondrite-normalized patterns) were also reported by Kitajima et al. (2008) for their smaller, submillimetric Malaitan alnöite zircons, with HREE contents > 1000 times chondrite. Similarly, calculated zircon compositions in equilibrium with OJP basalt (e.g. Mahoney et al., 1993) and a partial melt derived from the bimineralic clinopyroxene–garnet mantle xenoliths reported by Ishikawa et al. (2007) also contain HREE contents that are too high compared to those reported here (Fig. 4D). The calculated zircon composition in equilibrium with the asthenospheric diapiric melt derived from the depleted mantle source reported in Neal and Davidson (1989), the latter is based on garnet lherzolite xenoliths within minette (Ehrenberg, 1982) and kimberlite (Shimizu, 1975), has similar HREE contents but LREE abundances that are too low compared to those reported here (Fig. 4D). Alternatively, calculated zircon REE compositions in equilibrium with a melt derived from metasomatized garnet lherzolite, such as those present within the ~100 Ma old Nikos kimberlite (Schmidberger and Francis, 1999; Schmidberger et al., 2001) result in the most compatible chondrite-normalized pattern compared to those reported in this study (Fig. 4D). The two chondrite-normalized patterns for the metasomatized garnet lherzolites from the Nikos kimberlite represent average compositions for high (~1260 °C)- and low (~940 °C)-temperature suites, corresponding to depths of last equilibration between ~100 and ~180 km, respectively (Schmidberger and Francis, 1999). It is clear, therefore, that the very low REEs contents (Table S1) and chondrite-normalized patterns (Fig. 4D) for the Auluta, Faufaumela, and Kwainale megacryst zircons are most consistent with an origin via partial melting from a relatively deep (~100 km), metasomatized garnet peridotite mantle. This interpretation is consistent with the detailed petrographic and thermobarometric investigation of mantle xenoliths derived from the Malaitan alnöites (Ishikawa et al., 2004). The latter argue for the presence of variably metasomatized garnet lherzolites between ~30 and ~95 km and between ~100 and 110 km depths.

The well constrained negative correlation between ^{206}Pb/^{238}U ages and Zr/Hf ratios (and REE contents) for the zircons from the Auluta region (Fig. 9) may be attributed to crystallization from discrete partial melting events of a mantle source that was undergoing progressive metasomatism. The metasomatic agent invoked must be deficient in high field strength elements (HFSEs), such as a carbonatite-like fluid or melt since these are typically depleted in HFSEs (e.g. Nelson et al., 1988). For example, evidence for the Hf-depleted nature of zircons characterized by high Zr/Hf ratios (>70 to

253) derived from carbonatitic melts is documented in Proterozoic carbonatites from Ontario (Heaman et al., 1990), and the Phalaborwa and Mud Tank carbonatites (Hoskin and Ireland, 2000).

There is geological and petrographic evidence that suggest the presence of either carbonate-like melt/phase and/or CO_2 in the mantle beneath northern Malaita at the time of alnöite emplacement. For example, Allen and Deans (1965) report the occurrence of an alnöite breccia that immediately surrounds the alnöite pipe. The alnöite breccia is described as carbonated agglomerates consisting of rock and mineral fragments (~1 to 3 cm in diameter) set in a fine-grained matrix of pale greenish-white calcite (Allen and Deans, 1965). They provide micro-photographic evidence from the breccia of unaltered fragments of minerals (mica, pyrope garnet, opx, cpx) derived from the alnöite surrounded in a fine-grained calcite matrix. In addition, Nixon et al. (1980) describe the tuffs and breccias associated with the Malaitan alnöite as *fragmental* rocks with the coarseness and angularity of the fragments increasing from the tuffs to the breccias. The origin of the tuffs seems to have been highly turbulent and fluidized, whereas that of the breccias to be disruptive auto-brecciated; the coarsest breccias are alnöites veined with slickensided calcite (Nixon et al., 1980). Some of the fragments within the breccia are alnöite lapilli with a carbonate content >50%, which could have formed via silicate-carbonate liquid immiscibility (Nixon et al., 1980). Moreover, Nixon et al. (1980) postulated that the Malaitan alnöites possibly represent primary liquids derived from a pyrolite-type mantle formed by ~4% partial melting at depths >120 km at high CO_2 pressures.

In relation to a petrogenetic model arguing for discrete, low volume partial melting of a mantle source undergoing progressive metasomatism by carbonate or CO_2-dominated agent, the uniform Hf isotope data (Table S4) imply that the metasomatic agent and plume-like OJP mantle source are characterized by the same Hf isotope composition.

4.2. Protracted alkaline magmatism within the OJP: an analogy to cratonic lithosphere

Prior to the results presented in this study, the emplacement of the Malaitan alnöite pipes was believed to have occurred as a single magmatic event ~34 Ma ago based on a single ^{206}Pb/^{238}U date obtained by TIMS from a zircon megacryst (Davis, 1978). However, the in-situ U–Pb ages reported in Table S3 and shown in Figs. 5–7, and 10 indicate that alkaline magmatic activity occurred over a ~17 Ma interval. The distribution of the ^{206}Pb/^{238}U ages varies between
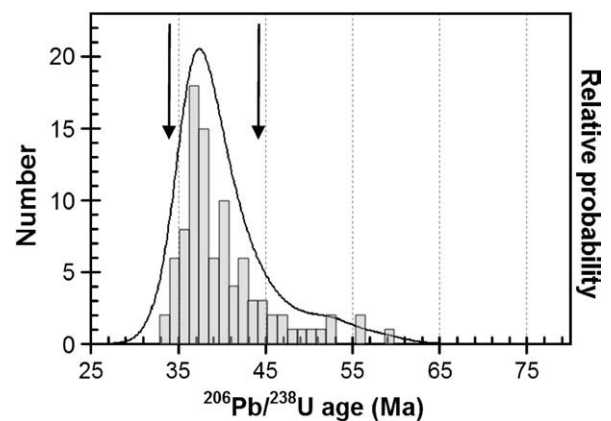

Fig. 10. Probability density plot exhibiting the distribution of calculated WM ^{206}Pb/^{238}U ages for Malaitan zircon megacrysts analyzed in this study (Table S3). The arrows indicate previous age determinations for a phlogopite grain from a mantle xenolith at 34 Ma (Ar–Ar; Kelley and Wartho, 2000), 33.9 Ma WM ^{206}Pb/^{238}U age for a single zircon megacryst from Malaita (Davis, 1978), and the 44.2 ± 0.2 Ma Ar–Ar age for basalts belonging to the younger series and Northern Malaita Alkalic Suite (NMAS; Tejada et al., 1996).

samples with the zircons from Kwainale recording a uniform age of 36.72 ± 0.49 Ma (Fig. 7).

Fig. 10 illustrates a probability density plot of the WM $^{206}Pb/^{238}U$ ages obtained in this study ($n = 94$ analyses; Table S3). The vast majority ($n = 87$, or ~93%) define ages that either overlap (given their associated uncertainties) or fall in between the U–Pb date of 34 Ma for the zircon megacryst from Malaita (Davis, 1978), and the 44.2 ± 0.2 Ma Ar–Ar age for basalts belonging to the younger series and Northern Malaita Alkalic Suite (NMAS; Tejada et al., 1996). The oldest WM $^{206}Pb/^{238}U$ age of 51.9 ± 2.6 Ma recorded by grain Z5 from the Faufaumela constitutes the bulk of the remaining analyses, and this age falls between the 44 Ma old age for the NMAS and the ~60 Ma old emplacement date for the San Jorge ophiolitic assemblage on the neighboring island of Santa Isabel and the ~60 Ma eruptions of OJP basalt on the neighboring island San Cristobal (Tejada et al., 1996).

The fact that a majority of the WM $^{206}Pb/^{238}U$ ages plot between 44 and 35 Ma (Fig. 10) may be interpreted to represent either secondary Pb loss ages from a precursor 45 Ma old emplacement event, or intermittent volcanic activity. However, given that the WM $^{206}Pb/^{238}U$ ages for the Auluta zircons show well constrained correlations with major and trace element compositions (Fig. 3), then these features are not supportive of the secondary Pb loss interpretation. Based on their chemical nature (low Pb, U, Th, and REE contents), large milli-to-centimeter size, and the cross-cutting relationship of the alnöite pipes with the lower section of the Mid-Eocene Haruta Formation (Petterson, 1995), the 52 Ma age for grain Z5 from Faufaumela clearly cannot represent an emplacement age. Therefore, the latter is interpreted to represent a cognate crystal that was later entrained by an eruptive, post Mid-Eocene emplacement event. As stated earlier, the megacryst zircons examined here were obtained from ilmenite gravel deposits, and therefore it is not possible to provide an exact geologic context for their U–Pb ages; i.e. whether the latter represent emplacement ages of undiscovered alnöite pipes or crystallization associated with discrete mantle melt events. In particular since the Auluta gravel sample was taken from a river that contains two known alnöite occurrences (Kwaikwai and an alnöite sill further upstream; Neal, 1986). However, given their very large size and lack of internal chemical heterogeneities, which has previously been interpreted to suggest a prolonged residence time at upper mantle conditions (e.g. Corfu et al., 2003), then our preferred interpretation is that the majority of the megacryst zircons examined here represent cognate crystals with a minimum emplacement age of ~35 Ma. The alkaline magmatic activity associated with the Malaitan alnöites and formation of the zircon megacrysts most probably resulted from discrete, melt extraction events that occurred over a ~17 Ma interval (between ~52 and ~35 Ma ago) from a *common* mantle reservoir undergoing progressive CO_2- or carbonatite-dominated metasomatism. A similar span of time (~17 Ma) was also recorded by centimeter-sized zircon megacrysts from the Monastery kimberlite, South Africa (Zartman and Richardson, 2005), since these yielded U–Pb ages between ~89 and ~106 Ma and hence their formation may also be attributed to a similar petrogenetic model. The fact that the zircons from Faufaumela do not show the same correlation between major and trace element chemistry and U–Pb ages could be attributed to the heterogeneous nature of the mantle source at the scale of partial melting.

There are numerous examples in the literature dealing with oceanic, plume-related basalt volcanism, which document the 'classic' and general trend of magma evolution from early tholeiite-dominated to late-stage alkaline magmatism (e.g. Hawaii, Clague, 1987). However, the post-erosional alkaline suite of rocks at Hawaii consists predominantly of basanite, nephelinite, and melilite nephelinite. To our knowledge, the occurrence of highly alkaline silica-undersaturated alnöite intrusions within the island of Malaita, emplaced within an intra-oceanic environment during the Oligocene, represents a unique situation on a global scale. The U–Pb ages reported here indicate that kimberlite-like melt events occurred over a prolonged period of time

(~17 Ma) at the southwestern edge of the OJP. This situation is analogous to the kimberlite magmatic activity spanning tens of millions of years that is well documented for several cratonic (continental) regions world-wide (e.g. South Africa, Smith, 1983; Zartman and Richardson, 2005; North America, Heaman and Kjarsgaard, 2000). Unfortunately, previous U–Pb age dating investigations of zircons associated with kimberlites that also report accompanying major and/or trace element data and Hf isotope compositions are scarce or non-existent. It is therefore difficult to determine whether the time interval in alkaline magmatism associated with major, continental kimberlite provinces is the result of a common mantle source undergoing discrete, low volume partial melting, or related to intermittent hot spot or plume activity. However, the mere fact that kimberlite-like magmatism in Malaita occurred over an extended period of time similar to that recorded for continental kimberlite/ carbonatite provinces suggests an analogous tectonic situation; i.e. one that involves interaction between an overlying, thick oceanic lithosphere associated with the OJP (~85 km; Neal et al., 1997) and upwelling CO_2- and/or carbonate-bearing melts derived from convecting asthenospheric mantle (Bell and Simonetti, 2010).

Recently, the presence of carbonatite liquid within the realm of the oceanic mantle has been argued on the basis of electrical conductivity results designed at upper mantle conditions (Gaillard et al., 2008), and experimental melt products conducted at high pressures (Dasgupta and Hirschmann, 2006). Recent studies have shown that carbonate phases are stable up to 10 GPa pressure and that partial melting of carbonated asthenospheric (peridotite) mantle at ~300 km depth can produce carbonatite liquid (0.03–0.3%; Dasgupta and Hirschmann, 2006). These carbonatitic liquids, if extracted from deep within the oceanic mantle, are an abundant source of metasomatic fluids highly enriched in incompatible elements leaving behind a vast depleted mantle residue (Dasgupta and Hirschmann, 2006).

Phase equilibrium investigations of amphibole–carbonate and phlogopite–carbonate (metasomatized) peridotite by Eggler (1989) indicate that primary alkaline silicate melts such as alnöites are derived at depths of ~100 km; in contrast primary kimberlitic melts are derived at deeper levels (~180 km). Haggerty (1989) stated similar conclusions with regards to the depth of melt generation based on a 'mantle metasomes' (Na + CO_2-rich and K + H_2O-rich metasomatic horizons) model in the upper mantle; in general kimberlites and lamproites are believed to form at depths >150 km, whereas alkali-rich melts such as alnöites are derived at depths between ~75 and ~100 km. The depths of the mantle metasomes are not fixed but will vary according to the rate of asthenospheric upwelling, which provides the heat and metasomatic agents to the overlying lithosphere (Haggerty, 1989). Thus, the absence of kimberlites *sensu stricto* at Malaita is most probably related to the fact that the lithospheric root lacks the appropriate thickness (i.e. >150 km). However, the mere fact that alnöite melts were produced in an oceanic environment gives some support to the notion that the formation of large igneous provinces, such as the Ontong Java Plateau and their possible accretion to the cratonic margins via subduction processes, may be an effective process for continental growth through geologic time (e.g. Mann and Taira, 2004).

5. Conclusions

A summary of the results and interpretations reported in this study are as follows:

1. Major and trace element data and Hf isotope measurements obtained for megacryst zircons from Auluta, Faufaumela, and Kwainale rivers of north central Malaita are consistent with derivation from a melt produced from a metasomatized garnet peridotite source that is characterized by an OJP-like Hf isotope composition.

2. Given their chemical nature (low Pb, U, Th, and REE contents), large milli-to-centimeter size, and lack of internal chemical heterogeneities, our preferred interpretation is that most of the zircon megacrysts examined here may represent cognate crystals that had a minimum emplacement age of ~35 Ma. Based on the cross-cutting relationship of known alnöite pipes with the lower section of the Mid-Eocene Haruta Formation, the 52 Ma age recorded by grain #Z5 from Faufaumela probably does not represent an emplacement age if it was derived from known alnöite occurrences. Given the thick rain forest cover of central northern Malaita, older alnöite intrusions may be present.

3. To our knowledge, the highly alkaline nature and ~17 Ma span of time for magmatism recorded by the Malaitan megacryst zircons are both unique features in the realm of oceanic volcanism worldwide. This situation is analogous to the span of alkaline magmatic activity associated with cratonic kimberlite/carbonatite provinces. Thus, this unique situation may be attributed to the anomalous combined thickness of at least 85 km for both the oceanic crust and underlying MORB-type oceanic lithosphere that is present in the southwest Pacific region. Phase equilibrium studies indicate that alnöite primary melts are derived from metasomatized upper mantle at pressures corresponding to ~100 to 150 km depth, which is consistent with the tectonic setting beneath the island of Malaita. In contrast, on-craton kimberlites are derived from deeper levels (~180 km) of thicker, older regions of metasomatized continental lithosphere. Hence, the protracted alkaline magmatic activity as recorded by the Malaitan megacryst zircons suggests that the OJP represents an analogy to cratonic mantle conditions.

Acknowledgements

Appendix A. Supplementary data

Supplementary material and data associated with this article can be found, in the online version, at doi:10.1016/j.epsl.2010.04.004.

References

Allen, J.B., Deans, T., 1965. Ultrabasic eruptives with alnöitic–kimberlitic affinities from Malaita, Solomon Islands. Mineral. Mag. 34, 16–34.

Armstrong, J.T., 1995. A package of correction programs for the quantitative electron microbeam X-ray analysis of thick polished materials, thin films, and particles. Microbeam Analysis 4, 177–200.

Bell, K., Simonetti, A., 2010. Source of parental melts to carbonatites — critical isotopic constraints. Mineralogy and Petrology 98, 77–89.

Belousova, E.A., Griffin, W.L., Pearson, N.J., 1998. Trace element composition and cathodoluminescence properties of southern African kimberlitic zircons. Mineral. Mag. 62, 355–366.

Clague, D.A., 1987. Hawaiian alkaline volcanism. In: Fitton, J.G., Upton, B.G.J. (Eds.), Alkaline Igneous Rocks. : Geol. Soc. Sp. Publ., 30. Blackwell Scientific Publications, Oxford, pp. 227–252.

Coffin, M.F., Eldholm, O., 1994. Large igneous provinces: crustal structure, dimensions, and external consequences. Rev. Geophys. 32, 1–36.

Coleman, P.J., 1965. Stratigraphic and structural notes on the British Solomon Islands with reference to the first geological map, 1962. British Solomon Islands Geological Records 2 (1959–1962), 17–31.

Corfu, F., Hanchar, J.M., Hoskin, P.W.O., Kinny, P., 2003. Atlas of zircon textures. In: Hanchar, J.M., Hoskin, P.W.O. (Eds.), Zircon — Reviews in Mineralogy and Geochemistry, 53. Mineralogical Society of America, Washington DC, pp. 469–500.

Currie, K.L., Knutson, J., Temby, P.A., 1992. The Mud Tank carbonatite complex, Central Australia — an example of metasomatism at mid-crustal levels. Contrib. Mineral. Petrol. 109, 326–339.

Dasgupta, R., Hirschmann, M.M., 2006. Melting in the Earth's deep upper mantle caused by carbon dioxide. Nature 440, 659–662.

David, K., Schiano, P., Allègre, C.J., 2000. Assessment of the Zr/Hf fractionation in oceanic basalts and continental materials during petrogenetic processes. Earth Planet. Sci. Lett. 178, 285–301.

Davis, G.L., 1978. Zircons from the mantle. US Geological Survey Open File Report 78–701, 86–88.

Eggler, D.H., 1989. Carbonatites, primary melts, and mantle dynamics. In: Bell, K. (Ed.), Carbonatites: Genesis and Evolution. Unwin Hyman, London, pp. 561–579.

Ehrenberg, S.N., 1982. Rare earth element geochemistry of garnet lherzolite and megacrystalline nodules from minettes of the Colorado Plateau province. Earth Planet. Sci. Lett. 57, 191–210.

Fujinawa, A., Green, T.H., 1997. Partitioning of Hf and Zr between amphibole, clinopyroxene, garnet and silicate melts at high pressure. Eur. J. Mineral. 9, 379–391.

Gaillard, F., Malki, M., Iacono-Marziano, G., Pichavant, M., Scaillet, B., 2008. Carbonatite melts and electrical conductivity in the asthenosphere. Science 322, 1363–1365.

Gladczenko, T.P., Coffin, M., Eldholm, O., 1997. Crustal structure of the Ontong Java Plateau: modeling of new gravity and existing seismic data. J. Geophys. Res. 102, 22,711–22,729.

Green, T.H., 1994. Experimental studies of trace-element partitioning applicable to igneous petrogenesis — Sedona 16 years later. Chem. Geol. 117, 1–36.

Haggerty, S.E., 1989. Mantle metasomes and the kinship between carbonatites and kimberlites. In: Bell, K. (Ed.), Carbonatites: Genesis and Evolution. Unwin Hyman, London, pp. 546–560.

Hanchar, J.M., Hoskin, P.W.O., 1998. Mud Tank Carbonatite, Australia, zircon. Soc. Lum. Micros. Spec. News. 10, 2–3.

Heaman, L.M., Bowins, R., Crocket, J., 1990. The chemical composition of igneous zircon suites: implications for geochemical tracer studies. Geochim. Cosmochim. Acta 54, 1597–1607.

Heaman, L.M., Kjarsgaard, B.A., 2000. Timing of eastern North American kimberlite magmatism: continental extension of the Great Meteor hotspot track? Earth Planet. Sci. Lett. 178, 253–268.

Hoskin, P.W.O., 1998. Minor and trace element analysis of natural zircon (ZrSiO$_4$) by SIMS and laser ablation ICPMS: a consideration and comparison of two broadly comparative competitive techniques. J. Trace and Microbeam Techniques 16, 301–326.

Hoskin, P.W.O., Ireland, T.R., 2000. Rare earth element chemistry of zircon and its use as a provenance indicator. Geology 28, 627–630.

Hoskin, P.W.O., Schaltegger, U., 2003. The composition of igneous zircon and igneous and metamorphic petrogenesis. In: Hanchar, J.M., Hoskin, P.W.O. (Eds.), Zircon — Reviews in Mineralogy and Geochemistry, 53. Mineralogical Society of America, Washington DC, pp. 27–62.

Hughes, G.W., Turner, C.C., 1976. Geology of Southern Malaita. Honiara: Ministry of Natural Resources. Geological Survey Division, Bulletin 2 80 pp.

Irving, A.J., Frey, F.A., 1984. Trace element abundances in megacrysts and their host basalts: constraints on partition coefficients and megacryst genesis. Geochim. Cosmochim. Acta 48, 1201–1221.

Ishikawa, A., Kuritani, T., Makishima, A., Nakamura, E., 2007. Ancient recycled crust beneath the Ontong Java Plateau: isotopic evidence from the garnet clinopyroxenite xenoliths, Malaita, Solomon Islands. Earth Planet. Sci. Lett. 259, 134–148.

Ishikawa, A., Maruyama, S., Komiya, T., 2004. Layered lithospheric mantle beneath the Ontong Java Plateau: implications from xenoliths in alnöite, Malaita, Solomon Islands. J. Petrol. 45, 2011–2044.

Jochum, K.P., Seufert, H.M., Spettel, B., Palme, H., 1986. The solar system abundances of Nb, Ta and Y and the relative abundances of refractory elements in differentiated planetary bodies. Geochim. Cosmochim Acta 50, 1173–1183.

Johnson, K.T.M., 1994. Experimental cpx/ and garnet/melt partitioning of REE and other trace elements at high pressures: petrogenetic implications. Mineral. Mag. 58A, 454–455.

Kelley, S.P., Wartho, J.-A., 2000. Rapid kimberlite ascent and the significance of Ar–Ar ages in xenolith phlogopites. Science 289, 609–611.

Kinny, P.D., Dawson, J.B., 1992. A mantle metasomatic injection event linked to late Cretaceous kimberlite magmatism. Nature 360, 726–728.

Kitajima, K., Ishikawa, A., Maruyama, S., Sano, Y., 2008. Nano-SIMS U–Pb zircons dating and geochemistry of from alnöite in Malaita, Solomon Islands. 9th International Kimberlite Conference Extended Abstract No. 9IKC-A-00329. 3pp.

Konzett, J., Armstrong, R.A., Sweeny, R.J., Compston, W., 1998. The timing of MARID metasomatism in the Kaapvaal mantle: an ion probe study of zircons from MARID xenoliths. Earth. Planet. Sci. Lett. 160, 133–145.

Lemarchand, F., Villemant, B., Calas, G., 1987. Trace element distribution coefficients in alkaline series. Geochim. Cosmochim. Acta 51, 1071–1081.

Ludwig, K., 2003. IsoPlot/Ex 3.00. Berkeley Geochronological Center Spec. Pub. 4.

Mahoney, J.J., Storey, M., Duncan, R.A., Spencer, K.J., Pringle, M., 1993. Geochemistry and geochronology of the Ontong Java Plateau. In: Pringle, M., Sager, M., Sliter, W., Stein, S. (Eds.), The Mesozoic Pacific. Am. Geophys. Union, Geophys. Monogr, 77, pp. 233–261.

Mann, P., Taira, A., 2004. Global tectonic significance of the Solomon Islands and the Ontong Java Plateau convergent zone. Tectonophysics 389, 137–190.

Mitchell, R.H., 1986. Kimberlites: Mineralogy, Geochemistry, and Petrology. Plenum, New York.

Miura, S., Suyehiro, K., Shinohara, M., Takahashi, N., Araki, E., Taira, A., 2004. Seismological structure and implications of double convergence and oceanic plateau collision of Ontong Java Plateau and Solomon Island arc from ocean bottom seismometer-airgun data. Tectonophys. 389, 191–220.

Neal, C.R. 1986. Petrogenesis of kimberlite-type intrusives in the south-west Pacific. Unpublished PhD Thesis, University of Leeds, UK.

Neal, C.R., Davidson, J.P., 1989. An unmetasomatized source for the Malaitan alnöite (Solomon Islands): petrogenesis involving zone refining, megacrysts fractionation, and assimilation of oceanic lithosphere. Geochim. Cosmochim. Acta 53, 1975–1990.

Neal, C.R., Mahoney, J.J., Duncan, R.A., Jain, J.C., Petterson, M.G., 1997. The origin, evolution, and ultimate fate of the Ontong Java Plateau, SW Pacific: evidence from exposed plateau basement on Malaita, Solomon Islands. In: Mahoney, J.J., Coffin, M.F. (Eds.), Large Igneous Provinces: Am. Geophys. Union, Geophys. Monogr., 100, pp. 183–216.

Nelson, D.R., Chivas, A.R., Chappell, B.W., McCulloch, M.T., 1988. Geochemical and isotopic systematics in carbonatites and implications for the evolution of ocean-island sources. Geochim. Cosmochim. Acta 52, 1–17.

Nixon, P.H., 1980. Kimberlites in the south-west Pacific. Nature 287, 718–720.

Nixon, P.H., Mitchell, R.H., Rogers, N.W., 1980. Petrogenesis of alnöitic rocks from Malaita, Solomon Islands. Melanesia. Mineral. Mag. 43, 587–596.

Palme, H., Jones, A., 2005. Solar system abundances of the elements. In: Davis, A.M., Holland, H.D., Turekian, K.K. (Eds.), Treatise on Geochemistry, vol. 1. Elsevier-Pergamon, Oxford, pp. 41–61.

Palme, H., O'Neill, H.S.T.C., 2005. Cosmochemical estimates of mantle composition. In: Carlson, R.W., Holland, H.D., Turekian, K.K. (Eds.), Treatise on Geochemistry, vol. 2. Elsevier-Pergamon, Oxford, pp. 1–38.

Petterson, M.G., 1995. The geology of north and central Malaita, Solomon Island. (Including Implications of Geological Research on Makira, Savo, Isabel, Guadalcanal, and Choiseul between 1992 and 1995). Publication of Water and Mineral Resources Division, Honiara, Solomon Islands: Geol. Mem., 1/95.

Petterson, M.G., Babbs, T.L., Neal, C.R., Mahoney, J.J., Saunders, A.D., Duncan, R.A., Tolia, D., Magu, R., Qopoto, C., Mahoa, H., Natogga, D., 1999. Geologic–tectonic framework of Solomon Islands, SW Pacific: crustal accretion and growth within an intra-oceanic setting. Tectonophys. 301, 35–60.

Richardson, W.P., Okal, E.A., van der Lee, S., 2000. Rayleigh-wave tomography of the Ontong Java Plateau. Phys. Earth Planet. Int. 118, 29–51.

Rock, N.M.S., 1986. The nature and origin of ultramafic lamprophyres: alnöites and allied rocks. J. Petrol. 27, 155–196.

Schärer, U., Corfu, F., Demaiffe, D., 1997. U–Pb and Lu–Hf isotopes in baddeleyite and zircon megacrysts from the Mbuji-Mayi kimberlite: constraints on the subcontinental mantle. Chem. Geol. 143, 1–16.

Schmidberger, S.S., Francis, D., 1999. Nature of the mantle roots beneath the North American craton: mantle xenolith evidence from Somerset Island kimberlites. Lithos 48, 195–216.

Schmidberger, S.S., Heaman, L.M., Simonetti, A., Creaser, R.A., Cookenboo, H.O., 2005. Formation of Paleoproterozoic eclogitic mantle, Slave Province (Canada): insights from in-situ Hf and U–Pb isotopic analyses of mantle zircons. Earth Planet. Sci. Lett. 240, 621–633.

Schmidberger, S.S., Simonetti, A., Francis, D., 2001. Sr–Nd–Pb isotope systematics of mantle xenoliths from Somerset Island kimberlites: evidence for lithosphere stratification beneath Arctic Canada. Geochim. Cosmochim. Acta 65, 4243–4255.

Skulski, T., Minarik, W., Watson, E.B., 1994. High-pressure experimental trace-element partitioning between clinopyroxene and basaltic melts. Chem. Geol. 117, 127–147.

Shimizu, N., 1975. REE in garnet and clinopyroxene from garnet lherzolite nodules in kimberlite. Earth Planet. Sci. Lett. 25, 26–32.

Smith, C.B., 1983. Pb, Sr and Nd isotopic evidence for sources of southern African Cretaceous kimberlites. Nature 304, 51–54.

Tejada, M.L.G., Mahoney, J.J., Duncan, R.A., Hawkins, M.P., 1996. Age and geochemistry of basement and alkaline rocks of Malaita and Santa Isabel, Solomon Islands, Southern Margin of Ontong Java Plateau. J. Pet. 37, 361–394.

Workman, R.K., Hart, S.R., 2005. Major and trace element composition of the depleted MORB mantle (DMM). Earth Planet. Sci. Lett. 231, 53–72.

Zartman, R.E., Richardson, S.H., 2005. Evidence from kimberlitic zircon for a decreasing mantle Th/U since the Archean. Chem. Geol. 220, 263–283.

Table S2. LA-ICP-MS Operating Conditions and data acquisition parameters

ICP-MS	
Type	Magnetic Sectorfield
Brand and model	Thermofinnigan Element2
Forward power	1235 -1250 W
Cool gas (Ar)	16.63 l/min
Auxilary gas (Ar)	0.94 l/min
Sample gas (Ar)	1.05 – 1.15 l/min
Carrier gas (He)	0.7 l/min
LASER	
Type	Nd:YAG
Brand and model	New Wave Research UP213
Wavelength	213 nm
Pulse duration	5 ns
Spot size	175 & 40 µm
Repetition rate	2 & 5 Hz
Nominal energy output	55% & 100%
Laser fluency	2 & 29 J/cm^2
Data Acquisition Parameters	
Resolution mode	Low
Data acquisition protocol	Time-resolved analysis
Scan mode	E-scan
Scanned masses	202, 204, 206, 207, 208, 232, 235, 238
Settling time	1 ms
Sample time	1 ms
Samples per peak	4
Number of scans	1000
Detector mode	Both for mass 238, analog for the remaining masses
Detector deadtime	13 ns
Background collection	30 s
Ablation time for age calculation	30 s
Washout	15 s
Standardisation and data reduction	
External standards used	NIST 612 (trace elements), Mudtank (U-Pb)
Reference standards used	91500 (trace elements), TEMORA (U-Pb)
Data reduction software used	GLITTER$^©$ (trace elements), in-house (U-Pb)

For quantification of trace element abundances, at the start of the analytical session the ICP-MS instrument parameters (i.e. gas settings, torch position, lens stack voltages) were optimized in solution mode using a 1 ppb multi-element standard. Typical ion yields for Li, In, and U for this solution were ~3 x 10^5, ~2 x 10^6, and 2.5 x 10^6 cps, respectively. Subsequent to ion beam optimization, a reference mass calibration was conducted; this was then followed by instrument shutdown and exchange of the wet plasma introduction system with the laser ablation sample introduction set-up. The He gas flow rate into the laser ablation cell was typically ~0.7 Lmin^{-1} and optimized prior to the zircon lasering by conducting line rasters with the NIST SRM 612 glass standard. Trace element concentrations (Table S1) were obtained using a 40 micron spot size, 5 Hz repetition rate, and 100% power output corresponding to an energy density of ~29 J/cm^2. The analytical protocol employed is similar to that outlined by Hoskin (1998), using ^{179}Hf as the internal standard (obtained from electron microprobe analyses; Table S1) and the NIST SRM 612 glass as the external standard. In-situ analyses typically consisted of a 1 minute measurement of the background ion signals followed by a 1 minute data acquisition of ion signals subsequent the start of the laser ablation. Data reduction and calculation of elemental abundances were conducted using the GLITTER$^©$ laser ablation software (Macquarie University). The accuracy of the method was verified with repeated analyses of the 91500 zircon standard (Wiedenbeck et al., 1995) and the trace element abundances obtained here (Table S1) are in very good agreement with those obtained in previous studies (e.g., Wiedenbeck et al., 1995; Hoskin, 1998; Hoskin and Schaltegger, 2003).

As outlined by Frei and Gerdes (2009), the Element2 is well suited for U-Pb age dating of accessory minerals due to its: (1) high sensitivity, i.e. 1 x 10^6 cps/ppb analyte as described above; (2) use of a discrete dynode secondary electron multiplier that has a 5 to 20 fold larger

linear dynamic range thus circumventing the need for gain calibrations between electron

multipliers and faraday collectors (e.g. Simonetti et al., 2008); and (3) relatively flat peak tops in

low resolution mode allowing multiple sampling on peak tops resulting in overall more precise

determination of peak intensities. The operating conditions and data acquisition parameters

employed here for the U-Pb age determinations (Table S2) are similar to those reported by Frei

and Gerdes (2009) and these are summarized below. The aperature beam delivery system of the

UP213 system was used and all data were acquired with single spot analyses employing a 175

μm spot size. The latter is much larger than that typically used for in-situ dating of zircons (20 to

60 μm); however, this was due to the relatively young age of the megacrystic zircons analyzed

and their derivation from a juvenile mantle source, which combine to give extremely low

contents of total Pb (Table S1). In order to minimize laser induced elemental fractionation

(LIEF) a repetition rate of 2 Hz was employed with a nominal energy output of ~55%,

corresponding to laser energy of ~0.025mJ/pulse and fluence of ~2 J/cm^2. Individual analyses

took ~75 seconds to complete with the first ~30 seconds for measurement of the background ion

signals, followed by 30 seconds of ablation, and 15 seconds of washout time. Prior to the start of

the data acquisition, the laser was fired for 20 seconds with the shutter closed in order to stabilize

laser output power. All measurements were conducted using electrostatic scanning (E-scan) with

the magnetic field resting at mass ^{202}Hg. The following ion signals were acquired: ^{202}Hg,

^{204}(Pb+Hg), ^{206}Pb, ^{207}Pb, ^{208}Pb, ^{232}Th, ^{235}U, and ^{238}U. All data were acquired on four samples per

peak with a sampling and a settling time of 0.001 seconds for every isotope. ^{202}Hg was measured

to monitor the ^{204}Hg interference on ^{204}Pb (using a ^{204}Hg/^{202}Hg value of 0.229883; Rosman and

Taylor, 1999). A common Pb correction was not applied; however, individual measurement

scans that recorded ^{204}Pb cps subsequent to the ^{204}Hg correction based on the ^{202}Hg ion signal

were simply rejected. In addition, the ages reported in this study (Table S3) are based on the weighted mean (WM) ^{206}Pb/^{238}U ratio due to the larger ^{206}Pb ion signals measured (compared to ^{207}Pb) and thus considered more robust. LIEF was monitored with the repeated laser ablation analysis of the Mudtank zircon (732 ± 5 Ma; Black and Gulson, 1978) as the external standard using a 'sample-standard bracketing' technique (e.g. Simonetti et al., 2005; 2006). The Mudtank zircon was chosen as the optimal standard due to its relatively young age and low Pb content of ~2 ppm (Black and Gulson, 1978), which comes close to the abundances in the Malaita zircons (<1 ppm) studied here (Table S1). A typical sequence of analyses consisted of 5 measurements of the Mudtank zircon both prior and subsequent the measurement of 10 unknowns. All uncertainties associated with the measurement of the ^{206}Pb/^{238}U ratios, including the external reproducibility associated with the repeated measurements of the Mudtank standard zircon (2σ standard deviation ~4%) are propagated by quadratic addition using the method outlined in Horstwood et al. (2003).

Given the relatively young age and low Pb contents of the megacrystic zircons investigated here, it proved difficult to find an adequate secondary zircon standard for intermittent analysis in order to test the accuracy of the protocol described here (especially given the large spot size used). However, three single grains of the well characterized Temora zircon standard were available and large enough to be ablated at 175 μm (Table S3). These three analyses yielded a WM ^{206}Pb/^{238}U age of 418.8 ± 8.6 Ma (2σ) and a concordia age of 416.9 ± 7.9 Ma (2σ), which both agree well with the accepted ^{206}Pb/^{238}U isotope dilution TIMS age of 416.8 ± 1.1 Ma (which includes spike calibration uncertainties; Black et al., 2003). Calculations of all WM ^{206}Pb/^{238}U ages and the weighted mean Hf isotope composition (Table S4) were determined with IsoPlot v3.0 (Ludwig, 2003).

In-situ Hf isotope determinations for the Malaitan zircon megacrysts were obtained using a Neptune *Plus* multi-collector-ICP-MS instrument coupled to a UP213 laser ablation system at the Thermo Fisher Scientific factory in Bremen, Germany; the results are listed in Table DR4. All ion signals were simultaneously measured on Faraday detectors (n=7), which monitored masses ^{172}Yb, ^{173}Yb, ^{175}Lu, ^{176}Hf, ^{177}Hf, ^{178}Hf, and ^{179}Hf. Zircons were ablated using a spot size of 80 μm, repetition rate of 5 Hz corresponding to an energy fluence of ~11 J/cm^2, which resulted in ^{177}Hf ion signals >1 volt. The isobaric interferences of ^{176}Yb and ^{176}Lu were monitored and corrected for using the ^{172}Yb/^{176}Yb ratio of 1.71085 and ^{176}Lu/^{175}Lu ratio of 0.02656 (Blichert-Toft et al., 1997), respectively, and applying an instrumental mass bias correction based on the ^{179}Hf/^{177}Hf ratio of 0.7325. Individual analyses typically consisted of a 15 seconds on-peak blank measurement followed by a 1 minute lasering interval for data acquisition purposes. Correction of ion signals for isobaric interferences, blanks, and instrumental mass bias were conducted using the Neptune *Plus'* time-resolved software. The accuracy of the method and data validation was verified by the repeated analysis of the Mudtank and 91500 zircon standards using the identical measurement protocol as that employed for the Malaitan megacrysts. The average ^{176}Hf/^{177}Hf and ^{176}Lu/^{177}Hf values listed in Table DR4 for both the Mudtank and 91500 zircon standards agree very well (given their associated uncertainties) with the recommended ratios (Table DR4) as reported by Woodhead and Hergt (2005) and Blichert-Toft (2008), respectively.